Delay Analysis of Multi-Hop Satellite-Terrestrial Networks with Hybrid RF/FSO Links

Fahad S. Alqurashi, Osama Amin, and Basem Shihada
Computer, Electrical and Mathematical Sciences & Engineering (CEMSE) Division,
King Abdullah University of Science and Technology (KAUST),
Thuwal, Makkah Province, Kingdom of Saudi Arabia
Email: {fahad.alqurashi, osama.amin, basem.shihada}@kaust.edu.sa

***Abstract*—Industry and academics have shown a strong interest in satellite-terrestrial networks combined with new technologies such as free-space optics (FSO). We propose a downlink satellite-terrestrial network solution combining FSO with site diversity and multi-hop hybrid radio-frequency (RF)/FSO links. Although the proposed network architecture is a cost-effective solution with wide coverage and immunity against different weather conditions, the multi-hop links can degrade its delay performance. Hence, we analyze the network dropping probability and latency to address the hop-count problem for various applications. We validated the derived network performance by Monte-Carlo simulation and showed that this setting could support ultra low latency applications such as medical applications with latency between 3-10 milliseconds, audio/video 2-50 milliseconds, and augmented reality 7-20 milliseconds. Also, the proposed network guarantees 98 % data delivery with 20 nodes.**

***Index Terms*—Satellite-terrestrial networks, delay analysis, site diversity, free-space optical (FSO), hybrid radio frequency (RF)/FSO, and queuing system.**

I. Introduction

Researchers from both industry and academia are studying satellite deployment to provide a seamless connection for unconnected and under-connected populations. In the same context, the continual requirement for high data rates to serve demanding applications has fueled the development of RF, such as mmW, and FSO communication technologies. FSO- and mmW-based systems operate at unlicensed bands with the ability to provide a broadband bandwidth up to a few Gbps at a low cost, and up to a few kilometers communication range [1]–[6]. The performance of FSO connections in outdoor setting is significantly impacted by the weather conditions such as fog, snow, and dust [7]. Also, other than the weather conditions, beam devegance and atmosphric turbulance can impact the FSO perofrmance. Notably, the performance of the mmW connections is also influenced by weather conditions, including rain and snow. Consequently, weather circumstances can decrease the link availability in each band. However, a hybrid approach can considerably enhance the link availability by ensuring that either the FSO or RF link is always accessible regardless of the weather situation [8].

Recent research on satellites utilizing FSO technology has attracted significant attention. FSO technology offers various benefits, including high data rate, cost-effectiveness, low power consumption, and a small footprint. However, the weather conditions and turbulence can significantly affect the end-to-end stability of the FSO links, which impose some challenges on using only an FSO link [9]. One way to mitigate these challenges is to utilize the sight diversity by establishing communication links with some ground stations that have stable connections [10]. Another way exploits the previously mentioned FSO technology benefits and sets hybrid RF/FSO links between the satellite and terrestrial stations. For example, in [11] and [12], the authors studied the end-to-end error and outage probabilities of a satellite to ground base station via a relaying high platform altitude using hybrid RF/FSO links. Although using a relaying communication between the satellite and the ground base station with the hybrid RF/FSO links, there is no effort to study multi-hop satellite to ground base stations with a hybrid RF/FSO solution. In this regard, analyzing the associated delay is necessary to evaluate the proposed network solution, which is imperative to be investigated in various communication networks [13]–[16].

In this paper, we consider point-to-multi-hop satellite to terrestrial base stations downlink scenario using hybrid RF/FSO terrestrial communication while applying sight diversity between the satellite and the ground base stations (BSs). Although the adopted architecture can overcome the coverage and link stability problems, the multi-hop architecture may increase the delay or increase the dropped packets, degrading the quality-of-service [17]. Hence, we need to investigate and analyze the delay and the dropping probability as the number of relays increases. Therefore, The contribution of this paper can be summarized as follows:

- We propose a cost-effective, high-data-rate, low-energy consumption network architecture using Satellite FSO technology and hybrid RF/FSO terrestrial links adopting the mmW band.
- We analyze the network delay using sight diversity to communicate with the ground base stations by solving the hop-count problem and defining the latency and the dropping probability.
- We study the network performance under different weather conditions such as fog and validate the theoretical results by Monte-Carlo simulation.

The rest of the paper is organized as follows. Section II provides the mathematical channel modeling for the FSO and RF bands. Section III presents the proposed network and its

performance analysis. Then the numerical results are discussed in section IV. Finally, Section V concludes the paper and highlights some observations.

II. Mathematical Channel Modeling

The general diagram of satellite-terrestrial multi-hop hybrid RF/FSO network is shown in Fig. 1-(a). The adopted network can mitigate two-main challenges of RF and FSO communication links, which are rain and fog scenarios Fig. 1-(b), respectively. In the following, we will define the employed channel models of both bands.

1) FSO channel modeling: The FSO receiver's instantaneous signal-to-noise ratio (SNR) per symbol is provided by [18]:

$$\gamma_{\rm FSO} = \bar{\gamma}_{\rm FSO} h_{\rm FSO}, \tag{1}$$

where $\bar{\gamma}_{\rm FSO}$ and $h_{\rm FSO}$ are the average SNR and fading gain of the FSO connection, respectively, with $E[h_{\rm FSO}]$ normalized to unity, and $E[.]$ denotes the expectation operator. Assuming that a phase-locked loop (PLL) is used to correct for phase noise in the received optical signal and that the local oscillator (LO) power is sufficiently strong to ignore thermal and background noise, the average SNR $\bar{\gamma}_{\rm FSO}$ may be obtained by [18]:

$$\bar{\gamma}_{\rm FSO} = \frac{2E_{\rm avg}\eta^2 P_{\rm LO} P_{\rm FSO} G_{\rm FSO}}{\sigma^2_{\rm FSO}} \tag{2}$$

where $E_{\rm avg}$, η, $P_{\rm LO}$, $P_{\rm FSO}$, $G_{\rm FSO}$, and $\sigma_{\rm FSO}$ denote, respectively, the average symbol energy, photodetector responsivity, LO power, average transmitted optical power, attenuation factor, and variance of shot noise, which is represented as additive white Gaussian noise (AWGN). The Beers-Lambert law determines the attenuation factor $G_{\rm FSO}$ (in dB) as $G_{\rm FSO} = \alpha_{\rm FSO} z$ [11], where $\alpha_{\rm FSO}$ signifies the weather attenuation coefficient (in dB/Km) and z denotes the connection distance (in Km). The fading gain over the FSO connection is defined as $h_{\rm FSO} = h_a h_b$ [19], where h_a denotes the Gamma-Gamma atmospheric turbulence-induced fading gain factor established in [20] and h_b denotes the Gaussian pointing error-induced fading gain factor defined in [21].

The probability density function (PDF) of $\gamma_{\rm FSO}$ can be found using the same method as in [19]:

$$f_{\gamma_{\rm FSO}}(\gamma_{\rm FSO}) = \frac{\xi^2 \gamma_{\rm FSO}^{-1}}{\Gamma(\alpha)\Gamma(\beta)} G^{3,0}_{1,3}\left[\frac{\xi^2 \alpha\beta\gamma_{\rm FSO}}{(\xi^2+1)\bar{\gamma}_{\rm FSO}} \mid \begin{matrix} \xi^2+1 \\ \xi^2, \alpha, \beta \end{matrix}\right] \tag{3}$$

where ξ is the ratio between the pointing error standard deviation σ_s given by $\xi = \omega_{eq}/2\sigma_s$[14] and the beam radius. Here, $\omega^2_{eq} = \omega^2_z \sqrt{\pi}\,\mathrm{erf}(\nu)/2\nu \exp\left(-\nu^2\right)$, where $\mathrm{erf}(.)$ is the error function and ω_z is the optical beam radius at distance z from the transmitter aperture and $\nu = \sqrt{\pi}D/2\sqrt{2}\omega_z$ with D is the photodetector diameter. ω_z is given by $\omega_z = \theta_0 z$, where θ_0 is the transmit divergence at $1/e^2$. In Eq. 3, $\Gamma(.)$ is the standard Gamma function and $G[.]$ is the Meijer G-function as defined in [[22], Eq. (9.301)] with α and β are the scintillation parameters. Assuming spherical optical wave propagation, α and β in Eq. 3 can be calculated is follows [20]:

$$\alpha = \left[\exp\left(\frac{0.49\chi^2}{\left(1+0.18d^2+0.56\chi^{\frac{12}{5}}\right)^{\frac{7}{6}}}\right) - 1\right]^{-1} \tag{4}$$

$$\beta = \left[\exp\left(\frac{0.51\chi^2\left(1+0.69\chi^{\frac{12}{5}}\right)^{-\frac{5}{6}}}{\left(1+0.9d^2+0.62d^2\chi^{\frac{12}{5}}\right)^{\frac{5}{6}}}\right) - 1\right]^{-1} \tag{5}$$

where χ^2 is the Rytov variance and defined as $\chi^2 = 0.5C_n^2 k^{7/6} z^{11/6}$, $d = \left(kD^2/4z\right)^{1/2}$, and $k = 2\pi/\lambda_{\rm FSO}$ is the optical wave number with $\lambda_{\rm FSO}$ is the optical wavelength.

By using [[23], Eq. (07.34.21.0084.01)] and integrating $f_{\gamma_{\rm FSO}}(\gamma_{\rm FSO})$ we simply can evaluate the cumulative distribution function (CDF) of $\gamma_{\rm FSO}$ as follows:

$$F_{\gamma_{\rm FSO}}(\gamma_{\rm FSO}) = \frac{\xi^2}{\Gamma(\alpha)\Gamma(\beta)} G^{3,1}_{2,4}\left[\frac{\xi^2\alpha\beta\gamma_{FSO}}{(\xi^2+1)\bar{\gamma}_{FSO}}\Bigg|^{1,\xi^2+1}_{\xi^2,\alpha,\beta,0}\right] \tag{6}$$

2) RF channel modeling: As shown in [24] the instantaneous SNR observed by the RF receiver can be evaluated as follows:

$$\gamma_{\rm RF} = \bar{\gamma}_{\rm RF} h^2_{\rm RF}, \tag{7}$$

where $h_{\rm RF}$ is the fading gain over the RF channel, $E\left[h^2_{\rm RF}\right]$ normalized to unity, and $\bar{\gamma}_{RF}$ is the average SNR of the RF channel. The average SNR $\bar{\gamma}_{\rm RF}$ is calculated as follows [24]:

$$\bar{\gamma}_{\rm RF} = \frac{E_{\rm avg} P_{\rm RF} G_{\rm RF}}{\sigma^2_{\rm RF}} \tag{8}$$

where $P_{\rm RF}$ is transmitted RF power, $\sigma^2_{\rm RF}$ noise variance assuming zero-mean circularly symmetric AWGN, finally $G_{\rm RF}$ is the average power gain of the RF channel. The average power gain $G_{\rm RF}$ can be given by the following [24]:

$$G_{\rm RF}[dB] = G_T + G_R - 20\log_{10}\left(\frac{4\pi z}{\lambda_{\rm RF}}\right) - \alpha_{\rm oxy}\, z - \alpha_{\rm rain}\, z, \tag{9}$$

where G_T, G_R, and $\lambda_{\rm RF}$ are respectively, denote the transmit antenna gain, receive antenna gains, and wavelength of the RF channel. α_{oxy} is attenuation caused by oxygen absorption and $\alpha_{\rm rain}$ is the rain attenuation. with RF bandwidth W and the noise power spectral density N_0 The variance of the noise in the RF channel is given by $\sigma^2_{\rm RF} = WN_0N_F$, where N_F is the noise figure of the RF receiver [24]. The fading gain $h_{\rm RF}$ across the RF channel follows the Nakagami-m distribution [25], which accurately replicates a broad range of practical line-of-sight (LOS) and non-LOS fading channels found in reality [26], [27]. It is straightforward to demonstrate that the PDF of $\gamma_{\rm RF}$ is provided by [26] using power transformations of random variables:

$$f_{\gamma_{\rm RF}}(\gamma_{\rm RF}) = \left(\frac{m}{\bar{\gamma}_{\rm RF}}\right)^m \frac{\gamma_{\rm RF} m - 1}{\Gamma(m)} \exp\left(\frac{-m\gamma_{\rm RF}}{\bar{\gamma}_{\rm RF}}\right). \tag{10}$$

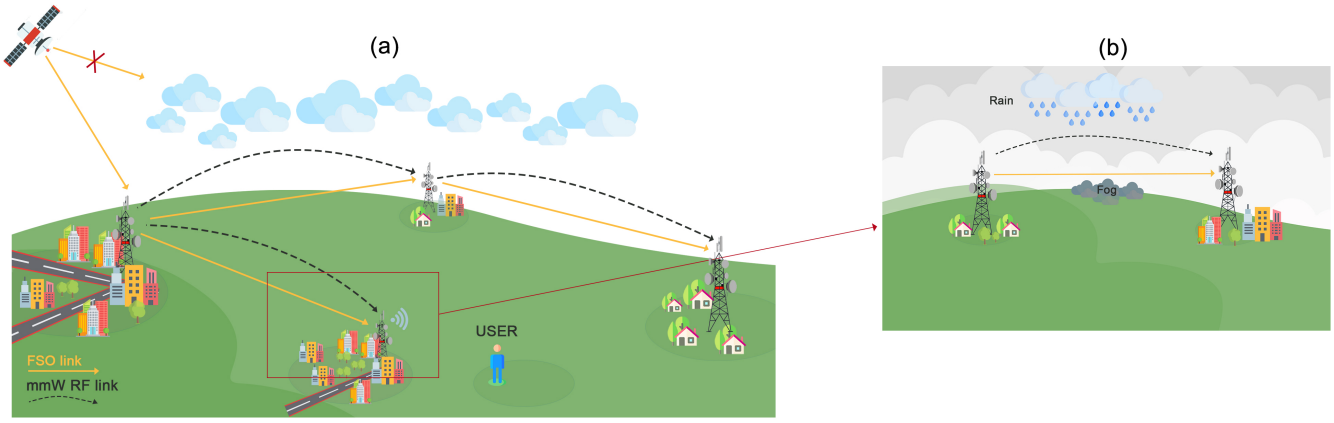

Fig. 1: (a) Illustration of FSO satellite to multi-hop hybrid RF/FSO terrestrial network. (b) Representation of the main challenges, Rain for RF band and Fog for the FSO band

By using [[23], Eq. (3.351 .1)], and some simple algebraic manipulations, the CDF of γ_{RF} can be expressed as:

$$F_{\gamma_{\mathrm{RF}}}\left(\gamma_{\mathrm{RF}}\right)=\frac{1}{\Gamma(m)}\gamma\left(m,\frac{m\gamma_{\mathrm{RF}}}{\bar{\gamma}_{\mathrm{RF}}}\right) \tag{11}$$

where $\gamma(\cdot,\cdot)$ is the lower incomplete Gamma function defined in [[23], Eq. (8.350 .1)].

III. Hybrid Satellite-Terrestrial Free Space Optical and Millimeter Wavelength Network

This section discusses the proposed network architecture along with the dropping and delay analysis used to assess its performance.

A. Network Architecture

The proposed network architecture consists of two main stages, satellite-to-ground BSs, and multi-hop ground BSs networks. We assume the satellite uses the sight diversity mechanism through an FSO channel to deliver the data to a ground BS. The sight diversity is adopted to overcome different weather conditions such as cloudy weather, which may limit some of the satellite-to-ground BSs connections causing a link failure. Thus, the satellite employs a scanning mechanism by sending a pilot message to ground BSs to sense the channel quality. Then, the satellite can send the data to the clearest path with the acceptable channel SNR, see Fig. 1-(a).

After delivering the data to a ground BS, it can reach the target destination via the appropriate multi-hop ground BSs. Each BS has the ability to operate in a dual band, mmW RF band or FSO band, based on the channel transmission quality. The RF and FSO channels are assumed to be periodically tested and the hybrid system can switch from one band to another.

The hybrid RF/FSO data transmission system is made of coherent/heterodyne FSO and RF data transmission subsystems. It is used to transmit data from one base station to another base station. The signal source generates a coded digital baseband signal, which is transformed to an analog electrical signal using an M-square quadrature amplitude modulation (QAM) electrical modulator in this hybrid system. M-QAM is commonly employed in high-rate data transfers via FSO and RF lines [28], [29]. The QAM signal will be broadcast through the FSO link or the RF link utilizing a mmW RF carrier, depending on the buffer size and channel condition, as detailed in Section III-B.

B. RF/FSO switching technique

Each base station is equipped with its own switching mechanism. To begin, we make the following assumptions:
1) Data is sent at the same rate via both FSO and RF lines.
2) The transmitter is aware of the channel's current status.
3) The arrival packets follows Poisson distribution.

The proposed switching technique is started with two main constrains, the threshold SNR γ_{TH} and the buffer size of the RF and the FSO links. For example, if a packet is arrived the switching will handover the packet to the FSO link, but if either the $\gamma_{\mathrm{TH-FSO}}$ or the buffer size is not satisfied, then the packets will transfer to the RF link. Additionally, if the $\gamma_{\mathrm{TH-RF}}$ or the RF buffer is full the packet will be dropped. The flowchart in Fig. 2 summaries the process of the proposed switching technique.

C. Dropping loss analysis

Using the proposed switching technique in III-B, there will be two possibilities to have dropping: (a) when γ_{RF} and γ_{FSO} both are lower than certain threshold, (b) or one buffer B_x is full and the other backup link has γ_x lower than the threshold ($x\in\{\mathrm{RF},\mathrm{FSO}\}$). The RF/FSO system can be represented as a two-dimensional discrete-time Markov chain and the packets will be served as first in first out (FIFO). Fig. 3 shows the two-state Markov chain (i,j), where i represent the RF link and j is related to FSO link. 1 means the γ_x constrain is not satisfied, and 0 is when the link is available and the buffer size below its maximum size. Then the dropping loss can be easily calculated as follows:

$$l_{\mathrm{RF}}=S(1,1)+S(1,0)\times a \tag{12}$$

$$l_{\mathrm{FSO}}=S(1,1)+S(0,1)\times b, \tag{13}$$

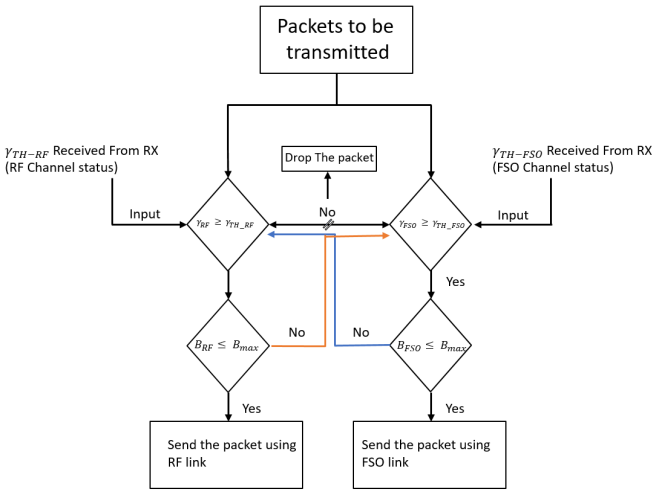

Fig. 2: Flowchart of the proposed switching technique

where a and b are $F_{\gamma_{\mathrm{RF}}}(\gamma_{\mathrm{TH-RF}})$ and $F_{\gamma_{\mathrm{FSO}}}(\gamma_{\mathrm{TH-FSO}})$, respectively, and they can be calculated using the CDFs of RF and FSO SNRs, i.e, (11) and (6), respectively. The so-called Erlang loss, $S(i)$ can be calculated as follows:

$$S(i) = \frac{\rho^i / M!}{\sum_{i=1}^{M} \rho^i / i!}. \tag{14}$$

The probability at steady state $S(i,j)$ can be recursively evaluated by linear equation set.

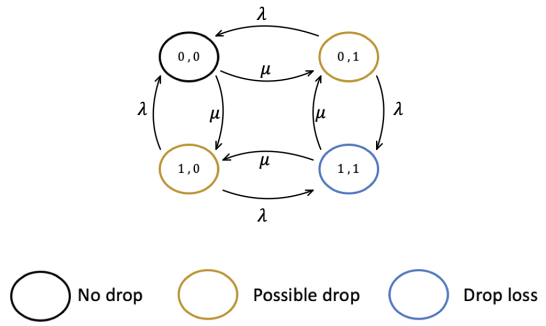

Fig. 3: Flowchart of the proposed switching technique

D. Delay analysis

First we will consider the wireless network as shown in Fig. 4 with K nodes each node represent RF/FSO hybrid BS, and the arrival rates of FSO and RF links, λ_{FSO} and λ_{RF}, are both equal λ. The packets arrives in an exponential inter-arrival times and distributed equally to the FSO and the RF links passing by the switching stage. As the distance between nodes and the user increases the response time, T_i will also increase in addition to the propagation delay τ_i. Therefore, the end-to-end delay, D, is expressed as follows,

$$D = \sum_{i=0}^{K} (T_i + \tau_i). \tag{15}$$

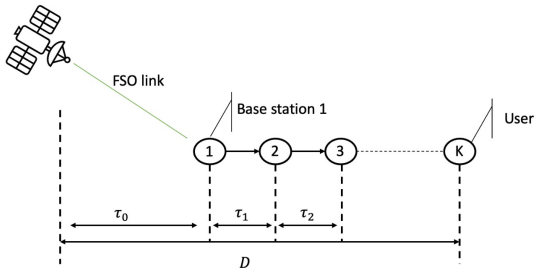

Fig. 4: Illustrations of having a satellite feeder and multiple base stations with RF/FSO system

Identifying the maximum number of nodes required to support a specific application is important to meet the operational conditions. Hence, it necessary to solve the maximum hop-count. Here, we first assign the required end-to-end response time that satisfies the quality of service, D_{QoS}, which varies from one application to another. For an arbitrary D_{QoS}, the maximum number of nodes, K^*, is given by:

$$K^* = \arg\max_{K} \left\{ \sum_{i=1}^{K} \overline{D_i} \leq D_{\mathrm{QoS}} \right\}, \tag{16}$$

where D_i is found from

$$D_i = \overline{W}_i + \sum_{i=1}^{K} \tau_i, \tag{17}$$

with $\overline{W}_i$ denoting the average waiting time at BS_i, which can be defined for either the FSO link or the RF as follows,

$$\overline{W}_i = \underbrace{(1-b)X_{i-\mathrm{FSO}}}_{\text{waiting time when using FSO link}} + \underbrace{b(1-a)X_{i-\mathrm{RF}}}_{\text{waiting time when using RF link}}, \tag{18}$$

where X_{i-x} is the service time at the i^{th} base station. Thus, If all base stations are identical, the maximum number on hop-count will be obtained as follows:

$$K^* \approx \frac{D_{\mathrm{QoS}}}{\overline{D_i}}. \tag{19}$$

IV. Numerical Results

In this section, we simulate the RF/FSO hybrid system as M/G/1 Markov chain and evaluate the dropping loss and the end-to-end delay. We assume RF channel fading severity of $m = 5$ and the FSO connection is most impacted by foggy weather. Moreover, we use the case of moderate and heavy foggy weather situation and moderate air turbulence with $C_n^2 = 5 \times 10^{-14}$ and no rain with RF rain attenuation $\alpha_{\mathrm{rain}} = 0$ dB/Km. Also, we assume a small zenith angle between the satellite and the ground BS, in order to reduce the attenuation and atmospheric turbulence at higher levels [10]. Regarding the transmission signal, we assume 16-QAM digital modulation with an average symbol energy E_{avg} is normalized to unity. γ_{TH-x} is chosen to be equal to 21 dB to satisfy a minimum target BER of 10^{-6}. Table I contains the necessary

parameters for the FSO and RF subsystems used to generate the numerical findings in this work.

TABLE I: Typical parameters of RF/FSO hybrid system

Parameter	Symbol	Value
FSO Subsystem		
Wavelength	λ_{FSO}	1550 nm
Oscillator Power	P_{LO}	10^{-2} W
Shot Noise Variance	σ^2_{FSO}	5×10^{-12}
Responsivity	η	0.5 A/W
Photodetector Diameter	D	20 cm
Transmit Power	P_{FSO}	15dBm
Transmit divergence at $1/e^2$	θ_0	2.5mrad
Jitter standard deviation	σ_s	30 cm
Link distance	z	1000 m
RF Subsystem		
Carrier Frequency	f_{RF}	60GHz
Bandwidth	W	250MHz
Transmit Power	P_{FF}	25dBm
Transmit Antenna Gain	G_{T}	43dBi
Receive Antenna Gain	G_{R}	43dBi
Noise Power Spectral Density	N_0	-114dBm/MHz
Receiver Noise Figure	N_{F}	5 dB
Oxygen Attenuation	α_{oxy}	15.1 dB/Km

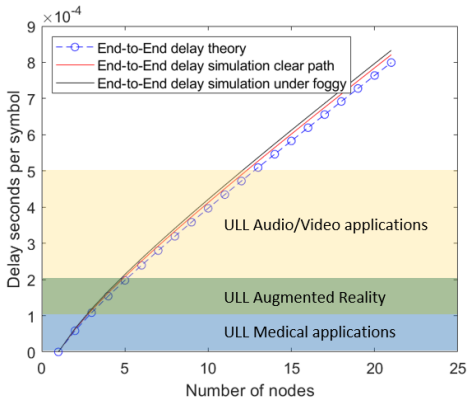

Fig. 5: End-to-end delay versus the number of nodes at $B_x = 10$ and with ULL proposed standards in [30]

In the first numerical example, we use Monte-Carlo simulation to validate the analytical findings with the same setting and buffer size $B_x = 10$. The simulation uses the SNR PDFs of the RF and FSO, which has been mentioned in section II. In Fig. 5, we study the end-to-end delay as a function of the number of relaying nodes, i.e., base stations. The "o" curve represents the theoretical end-to-end delay, which follows Eq. 19, while the black and red curves present the simulated end-to-end delay under foggy and clear weather situations, respectively. The figure shows that the Monte-Carlo simulation perfectly matches with the theoretical end-to-end delay. On another side, the end-to-end latency varies amongst applications, therefore one may specify a D_{QoS} constraint and determine the maximum number of hops. Specifically, we use some ultra low latency (ULL) real application examples, as shown in Fig. 5 [30] with blue, green, and yellow ranges. One can notice that no more than 3 nodes should be utilized for medical applications, which have a D_{QoS} ranges between 3-10 milliseconds. Regarding the audio/video (ULL 2-50 milliseconds) and augmented reality (ULL 7-20 milliseconds) applications the maximum hop-count are found to be 13 and 6 nodes, respectively. Here we can notice that the network in critical applications such as medical ones needs to be carefully designed with multiple points of presents from different locations to reduce the number of nodes.

In the second numerical example, we study the data transmission dropping probability versus the number of relaying nodes as illustrated in Fig. 6. The doted blue curve represents the theoretical dropping that follows the Erlang eq. (14). The "x" red curve is used to show the network stability limit with different routing protocol, which is studied in [31], Here, we choose a high stability limit with 98% packets delivery. The black and red curves show the dropping probability of the network in heavy fog and clear path, respectively. It is obvious to notice that as the number of nodes increases the dropping probability will also increase. However, The proposed network can guarantee packets delivery higher than 98% for clear path till almost moderate fog, but for heavy fog the maximum hop/nodes to satisfy the same constrain it needs to not exceed 7 nodes. Both numerical examples

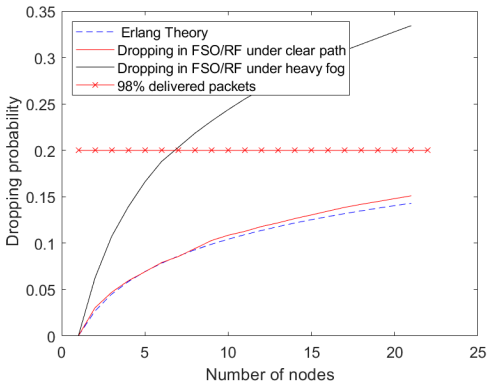

Fig. 6: Dropping probability versus the number of nodes (BS) $B_x = 10$

showed the case of heavy fog situation between nodes as shown in Fig. 5 and Fig. 6. In this case, the FSO band will not be available, but the latency remain the same because the packets will be transmitted through the RF band with the same data rates. On the other hand, if the hybrid links are asymmetric, where the data rates of the FSO and the RF are not the same, the performance is expected to degrade and the latency will increase. The main reasons behind this are the buffer size and bandwidth limitation. However, the dropping probability showed that there is an increase because the buffer of the RF band will be crowded and sometimes may lead to a drop. Finally, A table of comparison with current satellite to terrestrial networks is studied in Table II. The table showed that our proposed architecture has the lowest delay analysis compared to the analysis done in [32]–[34].

TABLE II: A delay comparison of multi-hop satellite to terrestrial networks

Ref.	Technology for Satellite to terrestrial	Technology for terrestrial multihop (BS-to-BS)	Max. delay (ms)
[32]	RF	RF	550
[33]	RF - 16 GHz	RF	250
[34]	RF - 20 GHz	RF - 14 GHz	ranges between 45 - 85
The proposed architecture	FSO - 1550 nm	Hybrid RF/FSO	38

V. Conclusion

In this paper, we proposed a downlink multi-hop satellite-terrestrial hybrid RF/FSO network to operate under different weather conditions and provide a cost-effective wide coverage network solution. We adopted a network with an M/G/1 Markov chain and switching techniques involving the SNR status and the buffer size. Based on a set of reasonable and practical assumptions, we proposed Markov chain models to analyze dropping loss and the latency and solve the maximum hop count. The model can be applied to a network with any number of nodes. Our proposed network can satisfy packet delivery higher than 98%. Also, by varying the required end-to-end delay, one can find the maximum hop count based on the required end-to-end delay. Finally, our proposed architecture has the lowest delay compared with the existing literature.

References

[1] L. C. Andrews, R. L. Phillips, and C. Y. Hopen, *Laser beam scintillation with applications*. SPIE press, 2001, vol. 99.

[2] F. Giannetti, M. Luise, and R. Reggiannini, "Mobile and personal communications in the 60 GHz band: A survey," *Wirel. Pers. Commun.*, vol. 10, no. 2, pp. 207–243, 1999.

[3] S. Dang, O. Amin, B. Shihada, and M.-S. Alouini, "What should 6G be?" *Nat. Electron.*, vol. 3, no. 1, pp. 20–29, 2020.

[4] H. Elayan, O. Amin, B. Shihada, R. M. Shubair, and M.-S. Alouini, "Terahertz band: The last piece of RF spectrum puzzle for communication systems," *IEEE Open J. Commun. Soc.*, vol. 1, pp. 1–32, 2020.

[5] W. Abderrahim, O. Amin, M.-S. Alouini, and B. Shihada, "Latency-aware offloading in integrated satellite terrestrial networks," *IEEE Open J. Commun. Soc.*, vol. 1, pp. 490–500, 2020.

[6] ——, "Proactive traffic offloading in dynamic integrated multi-satellite terrestrial networks," *IEEE Trans. Commun.*, vol. 70, no. 7, pp. 4671–4686, July 2022.

[7] A. Trichili, M. A. Cox, B. S. Ooi, and M.-S. Alouini, "Roadmap to free space optics," *J. Opt. Soc. Am. B*, vol. 37, no. 11, pp. A184–A201, 2020.

[8] F. Nadeem, B. Geiger, E. Leitgeb, S. S. Muhammad, M. Loeschnig, and G. Kandus, "Comparison of link selection algorithms for free space optics/radio frequency hybrid network," *IET Commun.*, vol. 5, no. 18, pp. 2751–2759, 2011.

[9] O. B. Yahia, E. Erdogan, G. K. Kurt, I. Altunbas, and H. Yanikomeroglu, "A weather-dependent hybrid RF/FSO satellite communication for improved power efficiency," *IEEE Wirel. Commun. Lett.*, 2021.

[10] E. Erdogan, I. Altunbas, G. K. Kurt, M. Bellemare, G. Lamontagne, and H. Yanikomeroglu, "Site diversity in downlink optical satellite networks through ground station selection," *IEEE Access*, vol. 9, pp. 31 179–31 190, 2021.

[11] S. Shah, M. Siddharth, N. Vishwakarma, R. Swaminathan, and A. Madhukumar, "Adaptive-combining-based hybrid FSO/RF satellite communication with and without haps," *IEEE Access*, vol. 9, pp. 81 492–81 511, 2021.

[12] R. Swaminathan, S. Sharma, N. Vishwakarma, and A. Madhukumar, "Haps-based relaying for integrated space–air–ground networks with hybrid FSO/RF communication: A performance analysis," *IEEE Trans. Aerosp. Electron Syst.*, vol. 57, no. 3, pp. 1581–1599, 2021.

[13] L. Xia and B. Shihada, "Power and delay optimisation in multi-hop wireless networks," *Int J. Control*, vol. 87, no. 6, pp. 1252–1265, 2014.

[14] I. Alabdulmohsin, A. Hyadi, L. Afify, and B. Shihada, "End-to-end delay analysis in wireless sensor networks with service vacation," in *IEEE Wirel. Commun. Netw. Conf. (WCNC)*, 2014, pp. 2799–2804.

[15] M. Alaslani, F. Nawab, and B. Shihada, "Blockchain in IoT systems: End-to-end delay evaluation," *IEEE Internet Things J.*, vol. 6, no. 5, pp. 8332–8344, 2019.

[16] M. AlAslani and B. Shihada, "Analyzing latency and dropping in todayâs internet of multimedia things," in *16th IEEE Annu. Consumer Commun. & Netw. Conf. (CCNC)*. IEEE, 2019, pp. 1–4.

[17] L. Xia and B. Shihada, "Max-min optimality of service rate control in closed queueing networks," *IEEE Trans. Automat. Contr.*, vol. 58, no. 4, pp. 1051–1056, 2012.

[18] M. Niu, J. Cheng, and J. F. Holzman, "Error rate performance comparison of coherent and subcarrier intensity modulated optical wireless communications," *J. Opt. Commun. Netw.*, vol. 5, no. 6, pp. 554–564, 2013.

[19] H. G. Sandalidis, T. A. Tsiftsis, G. K. Karagiannidis, and M. Uysal, "BER performance of FSO links over strong atmospheric turbulence channels with pointing errors," *IEEE Commun. Lett.*, vol. 12, no. 1, pp. 44–46, 2008.

[20] L. C. Andrews, "Laser beam propagation through random media," in *SPIE-Int. S. Opt. Eng.*, 2005.

[21] A. A. Farid and S. Hranilovic, "Outage capacity optimization for free-space optical links with pointing errors," *J. Light. Technol.*, vol. 25, no. 7, pp. 1702–1710, 2007.

[22] I. S. Gradshteyn and I. M. Ryzhik, *Table of integrals, series, and products*. Academic press, 2014.

[23] W. Research, "Mathematica edition: Version 8.0," *Champaign, Illinois: Wolfram Research Inc*, 2010.

[24] N. D. Chatzidiamantis, G. K. Karagiannidis, E. E. Kriezis, and M. Matthaiou, "Diversity combining in hybrid RF/FSO systems with PSK modulation," in *IEEE Int. Conf. Commun. (ICC)*, 2011, pp. 1–6.

[25] T. Rakia, H.-C. Yang, M.-S. Alouini, and F. Gebali, "Outage analysis of practical FSO/RF hybrid system with adaptive combining," *IEEE Commun. Lett.*, vol. 19, no. 8, pp. 1366–1369, 2015.

[26] M. K. Simon and M.-S. Alouini, *Digital communication over fading channels*. John Wiley & Sons, 2005, vol. 95.

[27] H. A. Suraweera, P. J. Smith, and J. Armstrong, "Outage probability of cooperative relay networks in Nakagami-m fading channels," *IEEE Commun. Lett.*, vol. 10, no. 12, pp. 834–836, 2006.

[28] B. T. Vu, N. T. Dang, T. C. Thang, and A. T. Pham, "Bit error rate analysis of rectangular QAM/FSO systems using an APD receiver over atmospheric turbulence channels," *J. Opt. Commun. Netw.*, vol. 5, no. 5, pp. 437–446, 2013.

[29] X. Lei, P. Fan, and L. Hao, "Exact symbol error probability of general order rectangular QAM with MRC diversity reception over Nakagami-m fading channels," *IEEE Commun. Lett.*, vol. 11, no. 12, pp. 958–960, 2007.

[30] A. Nasrallah, A. S. Thyagaturu, Z. Alharbi, C. Wang, X. Shao, M. Reisslein, and H. ElBakoury, "Ultra-low latency (ULL) networks: The IEEE TSN and IETF DetNet standards and related 5G ULL research," *IEEE Commun. Surv. Tutor.*, vol. 21, no. 1, pp. 88–145, 2018.

[31] M. M. Mahmoud, X. Lin, and X. Shen, "Secure and reliable routing protocols for heterogeneous multihop wireless networks," *IEEE Trans. Parallel Distrib. Syst.*, vol. 26, no. 4, pp. 1140–1153, 2015.

[32] H. Zhang and C. Wang, "Research on routing control with delay constraint based on contact plan for integrated satellite terrestrial network," in *IEEE 8th Int. Conf. Inform., Commun. and Netw. (ICICN)*. IEEE, 2020, pp. 155–159.

[33] Z. Ji, S. Wu, C. Jiang, and W. Wang, "Popularity-driven content placement and multi-hop delivery for terrestrial-satellite networks," *IEEE Commun. Lett.*, vol. 24, no. 11, pp. 2574–2578, 2020.

[34] D. Liu, J. Zhang, J. Cui, S.-X. Ng, R. G. Maunder, and L. Hanzo, "Deep learning aided routing for space-air-ground integrated networks relying on real satellite, flight, and shipping data," *IEEE Wirel. Commun.*, 2022.